 doi:10.20944/preprints202205.0256.v1

Research Article

Enhancement of neuroglial extracellular matrix formation and physiological activity of dopaminergic neural cocultures by macromolecular crowding

Andy N. Vo[1, #], Srikanya Kundu[1, #], Caroline Strong[1], Olive Jung[1], Emily Lee[1], Ming Jae Song[1], Molly E. Boutin[1], Michael Raghunath[2] and Marc Ferrer[1, *]

[1] National Center for Advancing Translational Sciences (NCATS), National Institute of Health (NIH), Maryland, USA
[2] Institute for Chemistry and Biotechnology (ICBT), Zurich University of Applied Sciences (ZHAW), Switzerland
# These authors contributed equally
* Correspondence: Marc Ferrer, PhD; NIH/NCATS; 9800 Medical Center Drive, Rockville, MD 208050 USA; marc.ferrer@nih.gov; Tel.: +1 (240) 515-4118

Abstract: The neuroglial extracellular matrix (ECM) provides critical support and physiological cues for the proper growth, differentiation, and function of neuronal cells in the brain. However, in most in vitro settings that study neural physiology, cells are grown as monolayers on stiff surfaces that maximize adhesion and proliferation, and therefore lack the physiological cues that ECM in native neuronal tissues provides. Macromolecular crowding (MMC) is a biophysical phenomenon based on the principle of excluded volume that can be harnessed to induce native ECM deposition by cells in culture. Here, we show that MMC using two species of Ficoll with vitamin C supplementation significantly boosts deposition of relevant brain ECM by cultured human astrocytes. Dopaminergic neurons co-cultured on this astrocyte-ECM bed prepared under MMC treatment showed longer and denser neuronal extensions, a higher number of pre ad post synaptic contacts, and increased physiological activity as evidenced by higher frequency calcium oscillation, compared to standard co-culture conditions. When the pharmacological activity of various compounds was tested on MMC-treated co-cultures, their responses were enhanced, and for apomorphine, a D2-receptor agonist, it was inverted in comparison to control cell culture conditions, thus emulating responses observed in in vivo settings. These results indicate that macromolecular crowding can harness the ECM-building potential of human astrocytes in vitro forming an ultra-flat 3D microenvironment that makes neural cultures more physiological and pharmacological relevant.

Keywords: Extracellular matrices, Macromolecular crowding, human iPSC derived astrocyte and dopaminergic neurons, drug testing

1. Introduction

The lack of physiological relevant and predictive preclinical models has limited the success rate for drug approvals [1, 2]. For most *in vitro* cellular models, cells are grown as two dimensional (2D) monolayers which lack the physiological presence of cues from the microenvironment coming from parenchymal and systemic cell-cell and cell-extracellular matrix (ECM) interactions [3, 4]. The ECM not only influences the mechanical stress experienced by the cells but also modulates their access to biological and chemical cues, such as growth factors and ions, thus regulating cell growth, migration, differentiation, and specific function [5]. In the brain, the ECM provides a microenvironment that regulates axonal guidance, synaptogenesis, and regulates maintenance of synaptic stability and repair following injury. Both neurons and astrocytes contribute to the neural ECM [6, 7],

 doi:10.20944/preprints202205.0256.v1

and the composition of the ECM depends on the developmental stage and region of the brain [8]. In late development, the perineuronal nets (PNNs) are macromolecular structures responsible for synaptic stability and are composed of hyaluronic acid complexed with chondroitin sulfate proteoglycans (CSPGs), such as aggrecan, veriscan, neurocan, and brevican, and the glycoprotein tenascin-R [9, 10]. In contrast, the basement membrane surrounding cerebral blood vessels is composed of collagen type IV, laminin, fibronectin, and heparan sulfate proteoglycans (HSPGs) [11, 12].

It would be desirable to recapitulate the native tissue ECM in *in vitro* cellular systems to them ensure physiological relevance [13]. However, spontaneous cellular ECM deposition in physiological amounts and composition is tardy to do in standard aqueous culture conditions [14]. The exogenous addition of isolated ECM components has been used to increase the activity of cells in *in vitro* neural cultures [15, 16]. For example, laminin coatings have been shown to increase neurite extension and increase in the complexity of neurites formed by neuronal stem cells, and more complex fetal brain extracellular matrices increased neuronal network formation in 3D bioengineered model of cortical brain tissue [16]. In native tissues, production, secretion, and deposition of ECM by certain cell types is a process regulated by mechanical, chemical, and physical cues from the microenvironment [17]. Macromolecular crowding (MMC) is both a biophysical effect and a novel tissue engineering technology based on the principle of excluded volume created by large macromolecules [14, 18]. Macromolecules surrounding cells create steric constrains that limit the volume in which relevant biomolecules and substances can be exchanged and diffuse in and out of the cellular surroundings. These crowding effects increase reaction rates and diffusion within the culture system [19], and for matrix-producing cells, induces deposition of matrix proteins in the cells immediate surroundings [18]. In the past decade, there has been growing interest in utilizing macromolecular crowding in *in vitro* cell cultures to improve their physiological relevance by facilitating disposition of native ECM secreted. Several macromolecules have been shown to act as crowders thereby inducing ECM deposition, including dextran sulphate (DxS), Ficoll 70 and 400 kDa (Fc 70/400), polyethylene glycol (PEG), and polystyrene sulphonate (PSS) [20]. Until now, the *in vitro* effects of MMC in inducing the cellular production and deposition of ECM in 2D monolayers cell cultures have been demonstrated in a variety of mesenchymal cells, namely fibroblasts, mesenchymal stromal cells, tenocytes [14] and epithelia (keratinocytes) [21].

Here, we demonstrate that MMC in human astrocyte cultures escalates the endogenous deposition of neural native-like ECM components, including Collage IV, Laminin (alpha1) and Fibronectin. We have developed a neural co-culture system using human iPSC-derived dopaminergic neurons (iDopas) and iPSC-derived astrocytes (iAstros). In our study design, an astrocyte cellular "bed" is first established for a week by treating cells with Ficoll 70/400 to induce ECM formation under MMC by the astrocytes. Afterwards, iDopas are added, and a co-culture system is established for two weeks. At that point, neural activity is measured using single cell calcium fluorescence microscopy with a transduced calcium GCaMP biosensor. Our data show that: 1) astrocytes produce brain-relevant ECM under MMC conditions; 2) neurons co-cultured on MMC-treated astrocytes show enhanced synaptogenesis, complex neurites network and calcium activity; and 3) pharmacological responses to compounds targeting dopamine receptors in MMC-treated dopaminergic and astrocytes co-cultures emulate those expected from *in vivo* data.

2. Materials and Methods

2.1. Astrocyte culture

Astrocytes were cultured in 96 well flat bottom plates (CellCarrier-96 Ultra, PerkinElmer, USA Waltham, MA) coated with 100µL/well of 0.083 mg/ml Growth Factor Reduced Matrigel (Corning, Corning, NY) in ice-cold DMEM (Corning, Corning, NY) and incubated for overnight at 4°C. Human induced pluripotent stem cell (iPSC)-derived astrocytes ("iAstros") (iCell Astrocytes Kit,01434 Cat#R1092, Lot#104345, 105136, 105152,

 doi:10.20944/preprints202205.0256.v1

105337) were obtained commercially from Fujifilm Cellular Dynamic International (CDI-Fujifilm, Madison, WI) and cultured according to vendor's protocol. Cells were gently thawed into astrocyte culture medium comprising DMEM, high glucose, GlutaMAX™ Supplement, pyruvate (Gibco, 10569) supplemented with 10% fetal bovine serum (Gibco, 16000) and 1X N2 supplement (ThermoFisher, 17502). The iAstros were then spun at 380 × g for 5 mins and counted in Countess II an automated cell counter (ThermoFisher Scientific) using trypan blue exclusion for viability. Cells with at least 95% viability were seeded at 13.3×10^3 cells per well in 96 well plate with 200 µl of astrocyte culture medium (effectively 4.0×10^4 cells/cm^2) after aspirating the supernatant DMEM used for coating. We considered the day of iAstro seeding as Day1 on our experimental timeline. iAstros culture were maintained at 37^{0}C in cell culture incubator under 5% CO_2 in astrocyte culture medium with 100% medium change in every alternate day for 7 days. All the experiments were performed in 3 technical replicate plates per group per plate and repeated independently in 3 biological replicate sets.

2.2. Macromolecular Crowding (MMC) treatment

24 hr after seeding the astrocyte, at Day2 the cultures were treated in four groups: 1) Control group: no MMC treatment; 2) "VitC" group: L-ascorbic acid (100µM) treatment; 3) "MMC" group: Ficoll70 (37.5mg/ml) + Ficoll400 (25mg/ml) treatment; and 4) "MMC+VitC" group: simultaneous Ficoll70 (37.5mg/ml) + Ficoll400 (25mg/ml) and L-ascorbic acid (100µM) treatment. A 100µM stock solution of L-ascorbic acid (Tocris Bioscience, 4055) was prepared in CDI astrocyte culture media for the VitC treatment. For MMC treatment a cocktail of 37.5mg/ml Ficoll PM70 (Millipore-Sigma, GE17-0310-50) and 25mg/ml Ficoll PM400 (Millipore-Sigma, GE17-0300-10) was prepared in astrocyte culture media. The solutions were then filtered through a 0.22 µm pore size syringe filter. As shown in flow chart (Figure 1), starting at Day2 of iAstros seeding, the treatments were introduced with a change of astrocyte medium. The control group always received 100% change of fresh astrocyte culture medium. MMC treatment were continued two more times at Day5 and Day7 while changing medium. At Day8, cultures were either fixed and stained for extracellular matrix deposition, or media was aspirated, and neurons were seeded on top of astrocytes.

2.3. Astrocyte-Neuron co-culture

Co-culture of astrocytes with neurons started on Day8 and continued until Day 22. Human iPSC derived Dopaminergic neurons ("iDopas") were procured from Fujifilm CDI, WI (iCell DopaNeurons,01279, Cat#R1032, C1028; Lot#102224, 105288, 102614) were seeded on the iAstros bed. Briefly, iDopas were gently thawed into CDI recommended dopamine culture medium consisting of iCell Neural Base Medium 1 (Fujifilm CDI, M1010) supplemented with 2% iCell Neural Supplement B (Fujifilm CDI, M1029) and 1% iCell Nervous System Supplement (Fujifilm CDI, M1031). Cells were spun down at 380 × g for 5 mins, counted in Countess II an automated cell counter from ThermoFisher, using trypan blue exclusion for viability. Because of variable viability between vials, the iDopas were processed with dead cell removal kit (Miltenyi Biotec, 130-090-101). Briefly, cells were spun again at 380 × g for 5 mins, medium aspirated completely and resuspended in Dead Cell Removal MicroBead solution in 1X Binding buffer (from the stock of 20X Binding buffer in the Kit) in sterile double distilled water (Fisher Scientific). 100µl of magnetic MicroBead solution was used per 10^7 total cells. The cell suspension incubated with the beads for 15 minutes at room temperature and then additional Binding buffer (1X) was added to make the final loading volume 500µl. The cell suspension was then loaded into MACS Column on MACS magnetic Separator from Miltenyi Biotec and allowed to pass through the column. The column was then thoroughly washed with 500µl of Binding buffer (1X) additionally 5 times. The flow-through live cells suspension was then resuspended in dopa culture medium and counted again for viability. At least 85% viable iDopas were then seeded as 66×10^3 cells per well on top of the ECM bed deposited by the

 doi:10.20944/preprints202205.0256.v1

mature iAstros culture, after carefully replacing the MMC with astrocytes medium. The wells were then filled with 200µl of dopamine culture medium and incubated at 37^{0}C in cell culture incubator with 5% CO_2. After 2 days of neuronal seeding, at experiment Day10, the dopamine cultural medium was 100% replaced with BrainPhys neuronal medium (STEMCELL Technologies, 05790) supplemented with 1X N2 (ThermoFisher, 175020-01), 1X B27 (ThermoFisher, 17504), 20 ng/ml of recombinant human BDNF (StemCell Technologies, No. 78005), 20 ng/ml of GDNF (StemCell Technologies, No. 78058), 1 µg/ml laminin (Gibco, 23017), 200 nM ascorbic acid (Tocris, 4055), and 1 mM cAMP (Tocris, 1141). The neural culture was maintained for 2 weeks with by-weekly media exchanges (50%) of BrianPhys medium. For the study of functional neuronal network activity, the co-culture were transduced with pAAV9.CAG.GCaMP6f.WPRE.SV40 (Addgene, 100844) at 10^6 MOI (Multiplicity of Infection) at Day10, at the same time that media was changed to Brainphys medium. Cultures were incubated for 2 weeks to allow the GCaMP6f protein to express.

2.4. Immunocytochemistry

Cell cultures were fixed with 4% paraformaldehyde for 30 mins at room temperature. Samples were then washed with PBS three times and blocked at room temperature on a shaker for 1 hr with 5% normal goat serum and 0.2% bovine serum albumin. 0.2% Triton-X was added to the samples that needed permeabilization for intracellular staining. Triton-X was excluded when staining for extracellular matrix. Primary antibodies were added (see Table 1 for dilutions), and samples were incubated at 4°C on a shaker, overnight. Samples were then washed with PBS three times. Secondary antibodies were added (see Table 1 for dilutions), and samples were incubated at room temperature on a shaker for 1 hr. Samples were then imaged on the Opera Phenix (Perkin-Elmer) under 20X water objective on confocal mode with respective filter setting according to the secondary antibody fluorescence.

Table 1. Primary and secondary antibodies and dilutions

Antibody Target (Clone)	Primary/secondary	Host & Clonality	Manufacturer & Catalog no.	Dilution
Collagen IV	Primary	Mouse monoclonal	Dako, M0785	1:200
Fibronectin	Primary	Rabbit polyclonal	Abcam, ab2413	1:200
GFAP	Primary	Rabbit polyclonal	Dako, Z0334	1:1000
Laminin (alpha1)	Primary	Rabbit polyclonal	Dako, Z0097	1:200
Microtubule-associated protein2 (MAP2)	Primary	Mouse monoclonal	Sigma, M4403	1:200
Tyrosine hydroxylase (TH)	Primary	Rabbit polyclonal	EMD Millipore, AB152	1:1000
Goat anti-mouse 555	Secondary		ThermoFisher, A28180	1:500
Goat anti-rabbit 647	Secondary		ThermoFisher, A27040	1:500
Goat anti-chicken 488	Secondary		Invitrogen, A32931	1:500

 doi:10.20944/preprints202205.0256.v1

2.5. Image analysis of Neural extensions and branching

Image analysis and quantitation of immunofluorescence signal from neural coculture was done using the software Harmony v5 (Perkin-Elmer). Because we did not include a nuclear cell marker for live cells image analysis, we used the GCaMP6f/FITC signal to identify neuronal cells. and for the fixed cell image analysis, we used Hoechst 33342 fluorescence for identifying the nuclei. We used the 'Find nuclei: Method B' algorithm using an area of >30μm² with common threshold 0.4, for locating nuclei. Used again GCaMP6f and TH primary antibody staining for live and fixed dopaminergic neuronal extensions identification, respectively. Then we applied the 'Find Neurites with CSIRO Neurites analysis 2' algorithm to mark the neurites with neurites segment from the preselected Nuclei. We calculated max neurites length per well/network, total neurites length per well/network and number of neurites branching per well/network. The data from 3 wells from each MMC treatment group, 3 biological replicates were summarized and plotted as bar graphs for comparison.

2.6. Live pre-synaptic vesicle tracking assay

The BioTracker 510 Green C4(FM1-43) Synaptic Dye (Sigma-Aldrich, SCT126) was used to measure newly form neurotransmitter vesicle at the pre-synaptic ends of live iDopa/iAstros co-cultures. The dye was made to its final concentration of 4μM in 50mM Tyrode solution and 200μl dye solution was added to wells after removing the media, incubated for 5 mins at room temperature, and imaged with a 10X confocal objective using FITC filter (λ_{Ex}=488nm and λ_{Em}=522nm) with a Phenix HCS reader. The raw fluorescent images were analyzed with ImageJ from 5 field of views per well, 3 wells per group from 3 biological replicates and normalized by respective background florescence (dF/F_0), and then plotted as bar plots to compare the amount of newly formed vesicles at the synaptic end as a scale for pre-synaptic plasticity.

2.7. Single-cell calcium flux imaging of transfected GCaMP6f neurons and astrocytes co-cultures

After 2 weeks of incubation of pAAV9.CAG.GCaMP6f.WPRE.SV40 transduction, GFP signal was measured from iDopas/iAstros coculture using a 10X water objective with Phenix Opera HCSS. First, the green laser (λ_{Ex}=488nm and λ_{Em}=522nm) was used to assess the fluorescence intensity of expressed GCaMP6f with a 60ms exposure time and 50% laser intensity. To measure basal live calcium flux over time, 300 frames of time-lapsed images were acquired over 180 sec period with 0.6 sec interval (1.6 frames/second). After basal GCaMP6f signal acquisition, drugs were added to culture wells and incubated for 5 mins, and the same acquisition process as above was used to acquire perturbations on the calcium flux.

The analysis of single cellular calcium fluorescence dynamics was as follows: The time-lapse images were stacked to provide maximum intensity projection using the Harmony v5.1 software (PerkinElmer) and transferred to the ImageJ image processing software. Then ROIs were automatically selected centering on the neuronal soma by the 'LC-Pro' plug-in in ImageJ by providing the ROI diameter (pixel) 30, frame rate (fps) 1.6 and an intensity cutoff threshold with a p-value 0.05. Finally, the raw intensity values of the calcium signal were extracted from selected ROIs. For the analysis, each ROIs data was transferred to 'Origin-Pro 9.0'(OriginLab). Single neuronal dynamics were quantified via the calcium signal peak frequency and peak amplitude. The peaks were detected over time by 'positive maximum intensity peak finding method' using 'batch peak processing algorithm', with second derivatives of individual ROI's raw fluorescence intensities (r.f.u.) as a change in fluorescence intensity from initial (dF) [22]. To improve the signal to noise ratio, the second derivatives of r.f.u. were used after thresholding the base line. The initial fluorescence level (F_0) for each ROIs was calculated by averaging the r.f.u. over full acquisition length and then the amplitude was normalized to dF/F_0 for each respective ROIs. Intentionally, the mean fluorescent intensity of the initial frames was not used as F_0. Because on every acquired time-lapsed image frame, calcium activity in terms of

 doi:10.20944/preprints202205.0256.v1

GCaMP6f fluorescence from scattered cells was observed. Completely silent calcium flux in any time point was never detected from the cultured cells. The peak frequencies (peak per sec) and mean peak amplitudes (dF/F_0) and mean peak width (dF/F_0) from each ROIs, minimum of 3 ROIs per well from 3 technically replicated wells per groups and 3 biologically replicated plates per experiments were plotted as bar graph. We repeated the same analysis for each drugs treated group.

For the generation of the correlation heat map among ROIs, the F/F_0 values for a region of interest (ROI) were exported to a text file titled ROI Normalized in Image J. This text file was converted to a csv file and uploaded into Python for peak detection analysis. The code for this analysis is publicly available on GitHub [URL: gist.github.com/25086]. Briefly: First, data from all identified ROIs was normalized such that the minimum F/F_0 value was equal to 1. Time series plots showing mean signal plus variability represented as 95% confidence interval were generated, along with heatmaps showing activity across every identified ROI, and a correlation matrix plotted as a heatmap representing correlation coefficients across all ROIs. The correlation matrix was used to describe how synchronous the calcium activity within the neural network across the well was, and a synchrony score was measured by calculating the average correlation coefficient across the matrix. Given that LC-Pro identifies different numbers of ROIs for each recording, we used a random sample generator to randomly choose 12 ROIs for peak detection analysis. To ensure this random sample reflected the population activity, we required the correlation score of the random sample to be within 5% of the correlation score of the population of ROIs.

2.8. Pharmacological perturbation of calcium dynamics in neural co-culture systems

We choose to assess the effects of three drugs targeting two receptors, dopamine and m-opioid receptors on the calcium dynamics of the iDopas+iAstros coculture system after MMC treatment: Apomorphine, a D2-receptor agonist; Metoclopramide, a D2-receptor antagonist, and Morphine, the μ-opioid receptor agonist. Each compound except for Morphine was tested at 10μM. Final concentration of Morphine was 15μM. Each compound was tested in three separates biological replicates, each with at least of 3 technical replicates. 10 mM solutions of the compounds in DMSO were diluted 1:100 in 1x PBS. 20μl/well were added except for Morphine, which was added 30μl/well, each time removing equal volume of medium from the well before adding the compounds. Drug treatment was done for 5 minutes before imaging.

2.9. Statistical analysis

Each bar graphs were plotted in GraphPad Prism 9.0 as mean±s.e.m. across 4 MMC treatment groups, Control, VitC, MMC, MMC+VitC. The pharmacological effects of drug treatment were shown side by side bar in a plot comparison. To establish the differences among the groups, we performed Two-way ANOVA test comparing each group's mean with every other group's mean using Turkey statistical hypothesis with 0.05 Family-wise alpha threshold in 95% confidence interval. The statistical differences were represented as * as $p<0.05$; ** as $p<0.01$; *** as $p<0.001$; **** as $p<0.0001$ and n.s. as no statistical difference.

3. Results

3.1. Macromolecular crowding treatment enhances deposition of ECM by cultured human iPSC-derived astrocytes

Mature astrocytes secrete and deposit a wide variety of proteoglycans and extracellular matrix proteins which impact the growth of astrocytes themselves and contributes to the development of neural microenvironment and networks *in vivo* [23]. The neural ECM includes various interwoven meshwork of fibrillar proteins including collagens, glycoproteins such as laminins, fibronectin, tenascins, and several classes of proteoglycans (heparan sulfate, chondroitin sulfate, dermatan sulfate, etc) [24-26]. To investigate

 doi:10.20944/preprints202205.0256.v1

whether MMC has an impact on the extracellular matrix deposition by iPSC derived human astrocytes (iAstros) *in vitro*, and subsequently, on the activity of neural network in cultures, we designed an experiment as outlined in Figure 1. iAstro were first seeded in wells of a 96-well microplate and treated for seven days with different combinations of MMC to induce ECM production, secretion and deposition. The treatments tested were Ficoll 70/400 as a macromolecular crowder, L-ascorbic acid ("VitC") [27], which regulates collagen synthesis and secretion, and a combination of Ficoll 70/400 and VitC ("MMC+VitC").

Figure 1: Schematic flow diagram of iPSC derived human Dopa and astrocyte neuronal coculture treated with varies combination of macromolecular crowding.

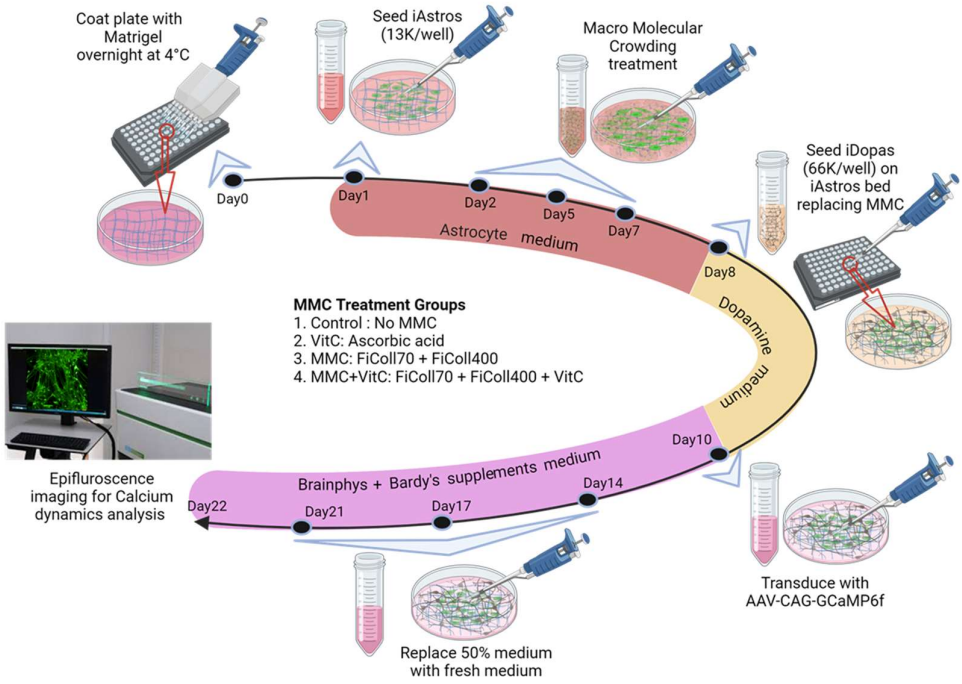

The flow diagram shows the timeline for the macromolecular crowding treatment on iPSC derived human neuronal coculture system. The PerkinElmer Ultra clear bottom 96 well plates were first coated with Matrigel at 4^{0}C, overnight, followed by seeding of iAstros (13K/well) the next day and incubation at 5% CO_2 at 37^{0}C. Four groups of macromolecular crowding testament were used: 1. Control: cells did not receive any crowding treatment; 2. VitC: cells received 100 µM of Vitamin C; 3. MMC: cells received cocktail of 37.5mg/ml Ficol70 and 25mg/ml Ficol400; 4. MMC+VitC: cells received same cocktail of Ficol70 and Ficol400 along with 100 µM of Vitamin C. With every 100% of astrocyte medium change, the cells received one of the four different treatments (n=3 wells/group; plates in duplicate). After 24 hrs of cell seeding (marked as day 1), cells were treated with MMC at days day 2, day 5 and day 7. At day 8, one culture plate was fixed with 4% PFA for immunohistochemistry study, and a duplicate plate was carried forward with the seeding of iDopas neurons (66K/well) on top of the treated astrocyte-ECM bed. The neurons are seeded after passing through dead cell removal process for a minimum viability of 85%. Caution was taken to replace (100%) astrocyte medium containing MMC with iDopas neuronal medium. After 2 days of iDopas seeding, at day 10 of our culturing timeline, the Dopa neuronal medium was 100% replaced with Brainphys with Bardy supplement for better neuronal growth. The coculture was then maintained for 14 more days at 37^{0}C with 5% CO_2. At day 22 all the functional assays performed.

 doi:10.20944/preprints202205.0256.v1

On day 8, the experimental plates were PFA-fixed for immunostaining, as mentioned previously. We selectively looked for the deposition of collage IV, fibronectin, and laminin (alpha1) because they are physiological relevant and antibodies are available for immunostaining and fluorescence microscopy. Representative images are shown in Figure 2a. We observed significant increases in the deposition of all three ECM proteins by the matured human astrocytes after 7 days of MMC treatment, as measured by the raw fluorescence intensity (r.f.u.) of respective immunostainings, when compared against the control/no treatment group. The MMC treatment singularly enhanced the collagen IV deposition 4-fold, (p<0.0001), and addition of VitC to the MMC boosted secretion of collagen IV to 7-fold (p<0.001), whereas VitC alone did not have any significant effect (Figure 2c) on collagen IV formation. Similar observations were also made for Fibronectin and Laminin (Figure 2d, 2e). Fibronectin was increased by 1.5-fold (p=0.002) with MMC and by 3.5-fold (p<0.0001) with MMC+VitC treatment (Figure 2d). For Laminin (alpha1), the deposition increased 1.5-fold (p<0.0001) for MMC and 2.6-fold (p<0.0001) for the MMC+VitC group (Figure 2e). None of the MMC treatments induced large changes in astrocyte numbers and maturity, after 7 days, as shown by GFAP staining (Figure 2f), compared to the control group.

Figure 2: Macromolecular crowding enhances extracellular matrices deposition by iAstros.

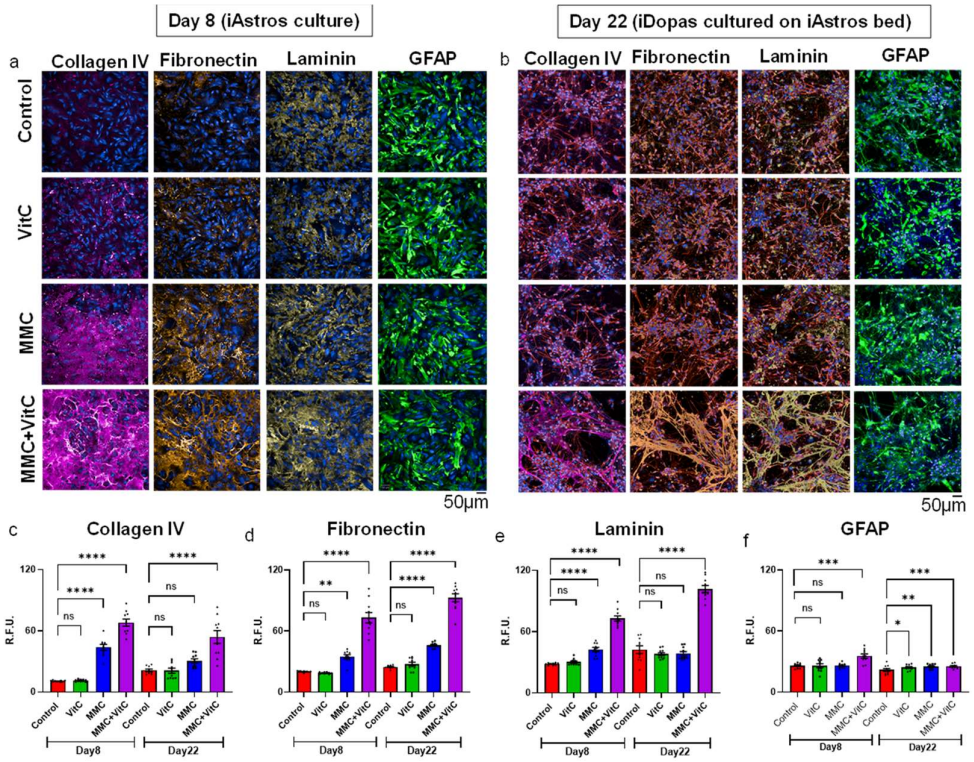

Comparative analysis of extracellular matrix deposition was performed by immunohistochemistry and fluorescence microscopy. All four groups, 1. Control (no macromolecular crowding); 2. VitC; 3.MMC (Ficol70+Ficol400); 4.MMC+VitC were stained with Goat anti mouse Collagen IV, Goat anti rabbit Fibronectin, Goat anti rabbit Laminin (alpha1) and Goat anti rabbit GFAP. (a) and (b) Representative images of extracellular matrices formation by iAstros monoculture at Day 8, and in the iDopas and iAstros neural cocultures at Day 22, respectively, with and without MMC treatments. (a) Macromolecular crowding of Ficol70 and Ficol400 combination (third row from top) induced deposition of collagen IV (magenta), fibronectin (orange), and laminin-alpha1 (yellow) at day 8, in comparison to the control group, and it was further enhanced with addition of VitC (bottom row). VitC alone could not make any significant difference. The astrocytes (GFAP staining) itself appeared healthy and matured in all four groups. (b) iDopa neurons were seeded on top of the treated astrocytes bed without disturbing the deposited extracellular matrices at day 8 and cocultured for another 14 days. At day 22 the matrices were checked with the same primary antibody staining mentioned above. The combination of Ficol70 and

 doi:10.20944/preprints202205.0256.v1

Ficol400 along with VitC group was again the most supportive of ECM secretion (bottom row). High density of web-like patterns was apparent by all three staining, Collagen IV (magenta), Fibronectin (orange) and Laminin (yellow), which was indicative of extended neurites projection of mature neurons, well established neuronal network with iAstro (GFAP staining). This web-like pattern was not profound on any other of its counterparts (top three rows). Nucleolus were stained with Hoechst in blue; Scale bar: 50μm. (c), (d) and (e) Bar graphs for the quantifications of deposited extracellular matrices density in terms of raw mean fluorescence (r.f.u.) intensity for Collagen IV, Fibronectin and Laminin, for each group. (f) r.f.u. of GFAP staining shows the healthy growth of iAstros after Day 8 and Day 22 in all four groups. The bar plots (n=3 wells/group; 3 biological replicates) showed all the extracellular depositions significantly enhanced after MMC+VitC treatment. Error bar: Standard error of mean; Statistical significance: Two-way ANOVA, *p<0.05, **p<0.01, ***p<0.001, ****p<0.0001, n.s.=not significant.

We next investigated whether the ECM formed by the iAstros, changed after addition of neuronal cells. For that, on day 8, iPSC derived human dopaminergic neurons (iDopas) were seeded on top of the ECM-iAstros bed and cultured for additional 2 weeks. On day 22 the iDopas+iAstros co-culture plate was PFA-fixed and repeated the same immunostaining procedure as above, for the assessment of Collagen IV, Fibronectin and Laminin (alpha1) deposition (Figure 2b). Collagen IV deposition increased in MMC+VitC group by 2-fold from the untreated group (p<0.0001), but there was 20% (p=0.0318) decrease in the amount of Collagen IV matrix under same treatment conditions after 2 weeks of neural co-culturing at Day22 compared to after mature astrocyte monoculture at Day 8 (Figure 2c). Fibronectin deposition increased by 2-fold (p<0.0001) in MMC and 4-fold (p<0.0001) in the MMC+VitC treatments group compared to control group on Day 22 (Figure 2d). There was 20% (p=0.0024) increase in fibronectin matrix from day 8, astrocyte monoculture to day 22, neural co-culture in the MMC+VitC treatment group (Figure 2d). Laminin (alpha1) deposition increased by 2.5-fold (p<0.0001) with the MMC+VitC treatments, but Laminin (alpha1) matrix did not change significantly from astrocyte monoculture to neural co-culture with any treatment's conditions (Figure 2e). After 2 weeks of neural co-culture, the astrocytes under all four treatment groups appeared matured by GFAP stanning, without significant change in r.f.u. (Figure 2f). Morphological comparison of the ECM scaffold formed before (day 8) and after (day 22) the addition of iDopas neurons, revealed that Fibronectin and Laminin (alpha1) appeared more mesh like and aligned with neural network in MMC+VitC treatment group compared to its control counterpart (Figure 2a and 2b, bottom row).

3.2. Macromolecular crowding treatment induces formation of neuronal extensions and branching

ECM has scaffolding functions to support cell attachment, growth and migration [28]. However, there is also evidence that ECM regulates many aspect of neural development, including morphogenesis of neural tubes [29, 30] and neocortex [31], and have a direct impact on the development of neural tissue [32]. With this in mind, we next sought to investigate whether the MMC induced ECM scaffold impacted any morphological features of the neuron-astrocyte co-cultures. We used immunostaining, fluorescence microscopy and quantitative image analysis techniques to first determine the number of dopaminergic neurons and astrocytes in our matured neural co-culture from all four treatment groups. We then measured neurite length, longitudinal coverage of total neurites per well, total area coverage of astrocytes, the average number of branching from the identified cell body as quantitative read-outs of neuronal morphology (Figure 3).

 doi:10.20944/preprints202205.0256.v1

Figure 3: Macro molecular crowding alters the phenotype of neural network.

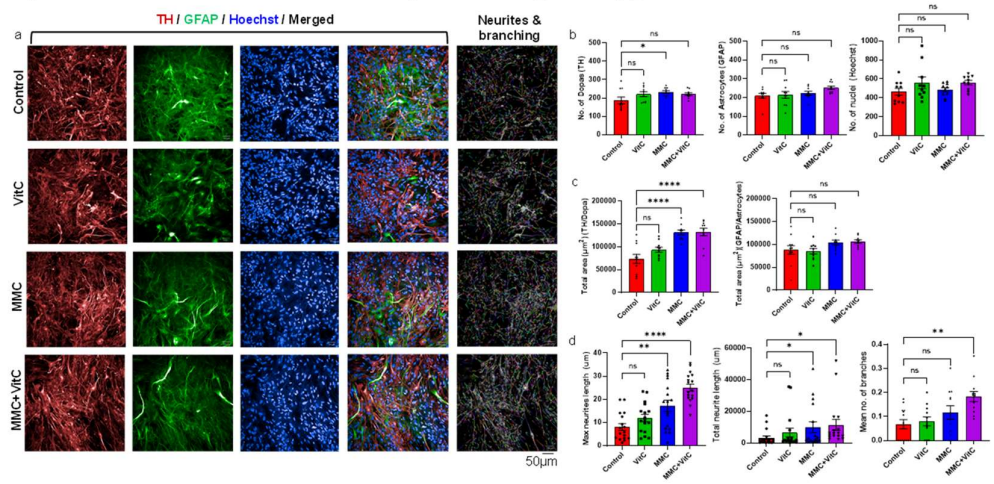

Image based analysis was used to determine morphological differences in terms of the neurite's length and number of neurites branching between all four macromolecular crowding groups, 1. Control; 2. VitC; 3. MMC; 4. MMC+VitC. (a) iDopas neurons and iAstros cocultures from all four MMC treatment groups imaged under 20X water immersion confocal microscope after immunostaining with cell specific primary antibodies. Anti-TH anybody (red) and anti-GFAP antibody (green) used to marked iDopas and iAstros cells respectively along with Hoechst 33342 (blue) for localization of the nucleus. Image analysis of neurites extension and branching pattern (multicolored) by Harmony 5v shows MMC+VitC group formed complex network with long and branched iDopas projections, compared to other groups (last column). (b) The 'find cell' algorithm was applied individually on each antibody staining, TH, GFAP and Hoechst 33342, and shows no significant changes in the number of cells per well, in each treatment group. (c) Quantitative analysis of total area coverage by the iDopas using TH staining and iAstros using GFAP staining per well indicates that with MMC and MMC+VitC treatments, the neuronal covered area increases without any changes in astrocyte covered area. (d) The 'find cell' algorithmic script for image analysis in Columbus software (PerkinElmer) providing ROI of ≥20µm² used to locate the neuronal cell body, and CSIRO Neurites Analysis 2 method was applied to mark the length along with segment/branches of neurites originated from those preselected cell bodies. Quantitative estimation of various parameters including maximum neurite length (µm), total neurites length (µm) per well, mean number of branches, compared between all four MMC treatment groups. The enhancement of extracellular matrices deposition by iAstro under MMC+VitC treatment supported iDopa neurons to form denser neuronal network with significantly increased neurites length, and total neurites coverage in the network with increased number of branches. The bar plots are mean±s.e.m. (n=3 wells/group; 3 biological replicates). Scale bar: 50µm; Statistical significance: Two-way ANOVA, *p<0.05, **p<0.01, ***p<0.001, ****p<0.0001, n.s.=not significant.

We first assessed whether MMC treatment affected the growth of astrocytes and dopaminergic neurons in terms of their cell counts. iAstros and iDopas were marked with GFAP (Figure 3a, green fluorescence) and Tyrosine Hydrolase (TH) (Figure 3a, red fluorescence) antibody-staining, respectively. The total cell nucleus was identified by Hoechst staining (Figure 3a, blue fluorescence). Our results revealed that there were no significant changes in the total or relative cell numbers of iDopas or iAstros the neural co-culture under any of the macromolecular crowding treatment conditions (Figure 3b). However, when the morphological features of the cells were analyzed, the data showed statistically significant increase in total area covered by iDopas under the MMC and MMC+VitC treatments by 78.16% (p<0.0001) and 79.44% (p<0.0001) respectively (Figure 3c). We did not observe any significant alteration in total area covered by the iAstros in neuron-astrocyte co-culture under any treatment conditions (Figure 3c). To assess whether the increase in iDopas total area coverage reflected an increased formation of neurite extensions in the co-culture, we used TH antibody staining for the fixed cells and green fluorescence signal from neural cultures transduced with a genetically encoded GCaMP6f biosensor to assess live neurite length and numbers of branches. The representative images from all four treatment groups are shown in Supplemental Figure 1. An image-based algorithm was

 doi:10.20944/preprints202205.0256.v1

used to first identify the cell bodies from the GCaMP6f green fluorescence signal and Hoechst staining for the fixed cells (Supplemental Fig 1b), and then neurite length and branching (Supplemental Fig 1c multicolor) were located and measured with image processing software. Combined quantitative analysis shown in Figure 3d indicated that the average longest neurites found within a well (Max neurites length) increased 2-fold (p=0.0012) under MMC alone and 4-fold (p<0.0001) under the MMC+VitC treatment. Total coverage of neurites (Total neurites length) increased by 3-folds (p=0.0474) in the MMC group and 10-fold (p=0.0124) in the MMC+VitC treatment group. Our MMC+VitC treatment also strengthened the neuronal network by increasing the average number of neurites branching by 3-fold (p=0.0055). We did not see any statistically significant change in neurite branching for MMC or VitC alone treatment groups.

3.3. Macromolecular crowding treatment induces synaptogenesis and synaptic plasticity

The neurites outgrowth observed led us to investigate the effect of MMC induced ECM secretion on the synaptic properties of the neural networks. Pre-synaptic activity was assessed with a synaptic dye which fluoresces green only when embedded into the newly formed transmitter vesicles inside the pre-synaptic ends of the neurons. This dye has a lipophilic tail at one end and other end is highly hydrophilic. In the aqueous phase the dye is non-fluorescence but during endocytosis following neuronal action potentials its trapped between lipid membrane of transmitter vesicles by its lipophilic tails and becomes intensely fluorescent. The fluorescent signal is proportional to the number of newly formed synaptic vesicles. We used this dye to trace the activity at the pre-synaptic end of our dopaminergic neurons for the four different treatment conditions. The representative confocal images shown in Figure 4a demonstrate an increase in live transmitter vesicle densit with MMC treatment. Quantitative analysis is shown in Figure 4b. Pre-synaptic fluorescence intensity (normalized by the background fluorescence) increased by 1.7-fold for MMC treatment (p=0.0017) and 2.4-fold (p<0.0001) for the MMC+VitC treatment group. We further look at the formation of post-synaptic terminals by immunostaining using PSD95 marker (magenta). Figure 4c show the representative confocal images of PSD95, co-stained with astrocytes marker GFAP, (Figure 4c, top row, green) or with neurites projections marker MAP2 (Figure 4c, bottom row, yellow). Combined quantitative analysis from both these double staining procedures (figure 4d) show an increase in PSD95 density (dF/F_0) by 20% (p=0.0113) with MMC treatment and by 80% (p<0.0001) with the MMC+VitC treatment, compared to the control group. The post synaptic density on astrocytes increased by 2.25-folds (p=0.0021) and 2.78-folds (p<0.0001) (Figure 4e) and the increase for neurons were by 1.58-folds (p<0.0001) and 1.95-folds (p<0.0001) (Figure 4f) after MMC and MMC+VitC treatment respectively, from their respective control group. Though the post-synaptic density enhanced more on astrocytes than neurons after the MMC treatment from its untreated counterparts. The neurite's outgrowth, boosted the overall post-synaptic connections on neurons substantially than astrocytes. We observed 27.34% and 33.71% PSD95 overlapped on GFAP while 74.27% and 91.53% overlapped with MAP2 in MMC and MMC+VitC groups (Figure 4e and 4f). Collectively, these data indicates that induced ECM secretion by astrocytes upon treatment with a macro molecular crowder together with L-ascorbic acid accelerated the development of mature complex neuronal network with improved synaptic connections.

 doi:10.20944/preprints202205.0256.v1

Figure 4: Macro molecular crowding enhances neuronal synaptic plasticity.

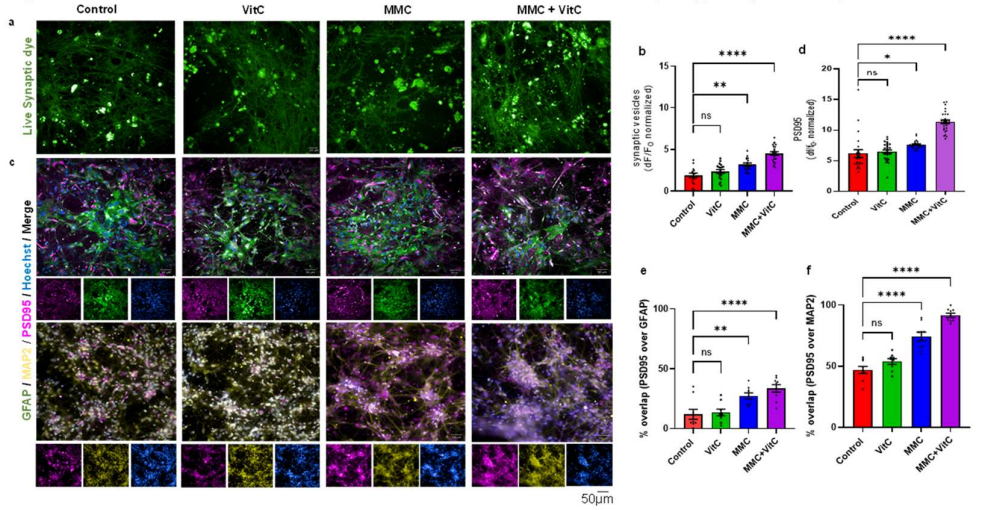

Macro molecular crowding with VitC strengthen the neural network by enhancing the formation of pre-synaptic vesicles and increasing the post-synaptic connections. Quantitative assessment of neuronal synaptic plasticity between all 4 MMC treatment groups performed in two ways. (a) Live cell imaging of newly formed active synaptic vesicles inside of pre-synaptic end of the neurons marked with BioTracker 510 Green C1 Synaptic Dye. After 10mins of incubation with the dye at RT, live cell epifluorescence images were captured under 10X water objective with FITC (λ_{Ex}=490nm; λ_{Em}=530nm) filter from all four groups of MMC, 1. Control; 2. VitC; 3. MMC; 4. MMC+VitC and represented here. The newly formed neurotransmitter vesicles at the cells synaptic terminals appeared as green-fluorescent puncta, as the lipophilic tail of the dye was embedded into the vesicle's membrane. (b) The mean raw fluorescence intensity (r.f.u.) normalized by their respective background fluorescence from each group (3 fields of view/well; n=3 wells/group from 3 biological replicates) quantitated with by ImageJ analysis software and plotted as a bar graph. (c) The postsynaptic density of neural network was estimated by immunostaining method with Goat anti mouse PSD95 primary antibody (magenta) from all four groups. PSD95, the post synaptic markers were co-stained with either Goat anti rabbit GFAP (green) or Goat anti rabbit MAP2 (yellow) to assess the presence of synaptic density with both iAstro and neurites respectively. Representative confocal images (10X water objective) from day 14 neuronal cultures from all four groups (6 wells/group) and measured mean fluorescent intensity of PSD95 (magenta) normalized by the background florescence from both sets of co-staining (3 field of views/well) was quantitated using ImageJ software and displayed as a bar plot (d). (e) and (f) show the bar plots for the percent area overlap of PSD95 over GFAP and MAP2, respectively. Scale bar: 50 µm; Error bar: standard error of mean; Statistical significance: Two-way ANOVA, *p<0.05 **p<0.01, ****p<0.0001, n.s.=not significant.

3.4. Macromolecular crowding treatment upregulates neural calcium dynamics

To assess whether the accelerated development of a mature neuronal network with improved synaptic connections seen in MMC+VitC treatment translated into functional modulation of neural activity, we measured calcium dynamics using single cell fluorescence imaging by expression a genetically encoded GCaMP6f biosensor in the co-culture. Representative confocal images of GCaMP6f activity from all four treatment groups are shown in Figure 5a. The oscillations of calcium waves (dF/F_0) from randomly chosen four example traces from each experimental group are shown in Figure 5b. Figure 5c is the heat map representation of the collective ROIs from respective treatment groups over time. Each row of the heat map represents single cell' (ROI) activity over time. The blue to yellow color scale in Figure 5c indicates the increases in amplitude as dF/F_0. The peak frequencies (peak per sec), mean peak amplitudes (dF/F_0) and mean peak width (dF/F_0) were calculated for each ROIs, minimum of 3 ROIs per well from 3 technically replicate wells, per 3 biologically replicates plotted as bar graphs (Figure 5e). The data shows that there were significant increases in calcium peak frequency by 30% (p=0.01), 50% (p=0.0001) and 70% (p<0.0001) in the VitC, MMC and MMC+VitC treatments, respectively. We did not observe statistically significant changes in peak amplitude and peak width between the different treatment groups because of scattered peak property values. We also assessed

 doi:10.20944/preprints202205.0256.v1

the synchronicity of single cellular calcium dynamics within network by plotting a correlation heat map of ROIs vs ROIs in Figure 5d, and calculated a correlation score within group, shown as bar plots in Figure 5f, to statistically compare synchronicity between groups. The color gradient from dark to light brown indicates the synchronicity from -1 to +1. Synchronicity in spontaneous calcium oscillations per cell is a measure of overall network' functional dynamics of neural cultures. The correlation heat maps display overlap in peak frequency between single neuron (ROIs) calcium oscillations. We observed 2.71% and 7.61% lower synchronicity in the calcium oscillations with MMC (p=0.0478) and MMC+VitC (p<0.0001) treatment respectively, compared to the untreated group.

Figure 5: Macro molecular crowding influences upregulation of calcium flux in neural co-cultures.

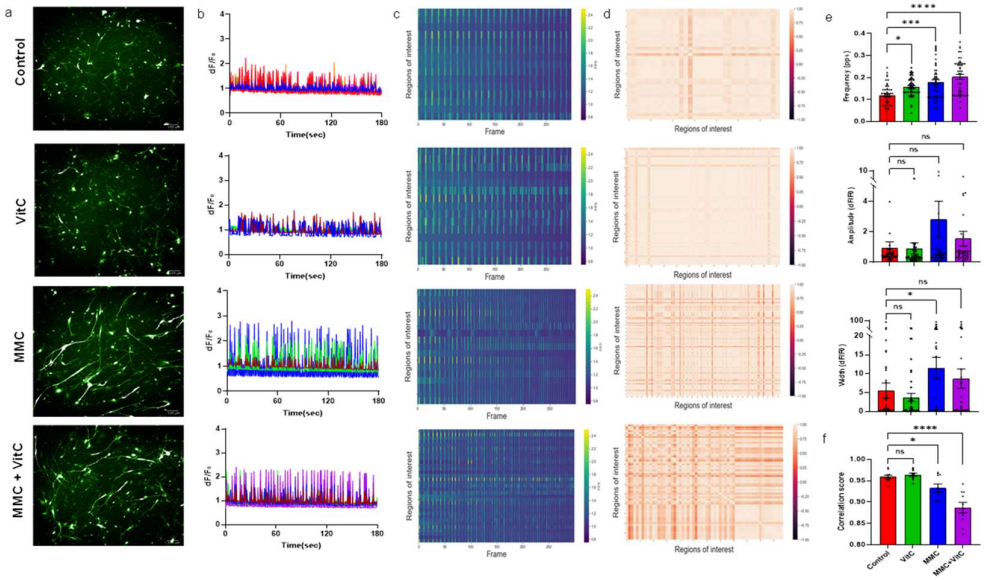

We measured imaged-based single cell calcium flux with transfected AAV-CAG-GCaMP6f the neural co-culture system as an indicator of the functional dynamics of its network activity. (a) Representative epifluorescence (10X water objective) images of iDopas+iAstros co-culture transfected with AAV6-CAG-GCaMP6f. The expression of GCaMP6f in the neuronal network is shown in green FITC (λ_{Ex}=490nm; λ_{Em}=530nm). (b) The representative fluorescence traces from single cell neuronal calcium dynamics over time, from each of the four treatment groups, are shown. A series of 300 time-lapsed images were captured over a period of 180 sec with 0.6 sec interval and single cell calcium flux (dF/F_0) were estimated by 'LC-Pro' plug-in in 'ImageJ' as described in method section. (c) The frequency of the calcium peaks from 50 individual neurons (Region of Interest) over time (frames) were also plotted as a heat map with the increasing amplitude from 0.8 F/F_0 as blue to 2.4 F/F_0 as yellow. (d) Correlation plots are shown as heat maps for the 50 cells/ROIs against each other. Color gradient from darker brown to lighter brown showed in color scale as negative 1 to positive 1 correlation, indicating the unsynchronized to perfectly synchronized calcium spiking activity. (e) Quantitated calcium peak properties, peak frequency (pps), peak amplitude (dF/F_0), and peak width (dF/F_0) from 9 wells (n=3 wells/group, 3 biological replicates) represented as bar plots. (f) Bar graph of correlation scores. Scale bar: 50µm; Error bar: standard error of mean; ; Statistical significance: Two-way ANOVA, *p<0.5, **p<0.1, **p<0.01, ***p<0.001, ****p<0.0001, n.s.=not significant.

3.5. Macromolecular crowding treatment promotes pharmacological responses that emulate those seen in vivo

We further explored whether the differences in neural activity seen for the MMC treated groups translated into more relevant pharmacological responses that emulate *in vivo* data. We chose three drugs targeting the D2 receptor on iDopas neurons: Apomorphine, a D2-receptor agonist; Metoclopramide, a D2-receptor antagonist; and Morphine, a µ-opioid receptor agonist. On Day 22, the single cell calcium fluorescence was first acquired (Figure 6a, 6b, 6c, empty columns) for each neural co-culture and then compounds

 doi:10.20944/preprints202205.0256.v1

(individually) were added to each well, incubated for 5 min, followed by repeat acquisition of single cell calcium fluorescence (Figure 6a, 6b, 6c, filled columns). The top row of Figure 6a, 6b and 6c showed bar plots for the calcium peak frequencies before (empty columns) and after (filled columns) the addition of Apomorphine, Metoclopramide and Morphine respectively, for the four MMC treatment groups. The detailed calcium peak traces and analysis of each individual drug treatment are presented in Figure S2, S3 and S4 for Apomorphine, Metoclopramide and Morphine, respectively. The graphs at the bottom row represent the % change in peak frequency [(drug-no drug)/no drug] for each compound treatment, in each MMC treatment group.

Figure 6: Pharmacological perturbation of neural calcium dynamics on macro molecular crowding-treated neural co-cultures.

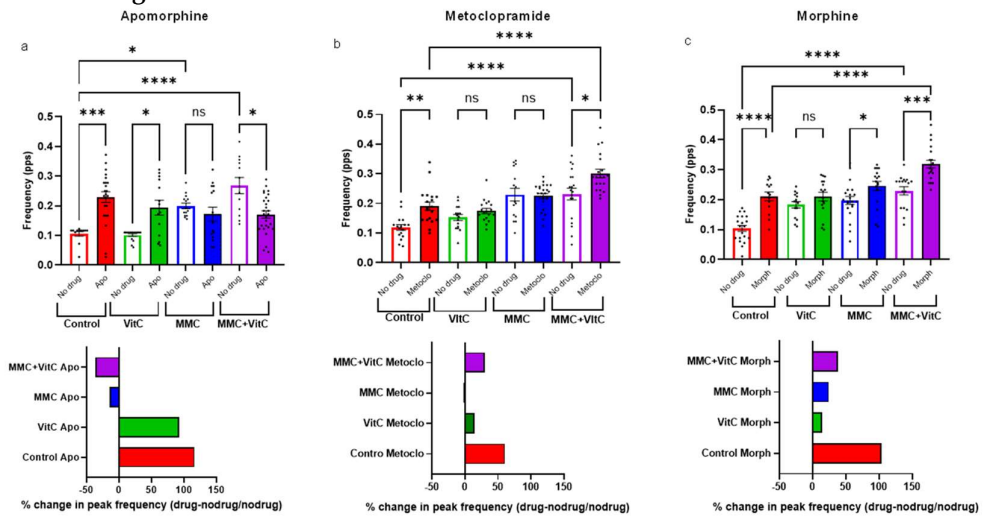

Pharmacological perturbation on the single cell fluorescence calcium dynamics with a (a) D2-receptor agonist (Apomorphine); (b) D2-receptor antagonist (Metoclopramide); and (c) μ-opioid receptor agonist (Morphine), after MMC treatment on iDopa+iAstro co-culture system. Top row represents the calcium peak frequency (pps) bar plots comparing before and after pharmacological interventions in all 4 MMC treatment groups. Bottom row shows the % change in peak frequency after pharmacological agent's interventions from the corresponding no drug basal level. Error bar: standard error of mean from 9 wells (n=3 wells/group, 3 biological replicates); Statistical significance: Two-way ANOVA, *p<0.5, **p<0.1, **p<0.01, ***p<0.001, ****p<0.0001, n.s.=not significant.

For Apomorphine, we observed a ~2-fold increase over non-compound treated in calcium peak frequency for the control (p=0.0002) and VitC groups (p=0.0215), but a decrease of 40% (p=0.0491) in the MMC+VitC group (Figure 6a), and there was not statistical change in MMC treatment group. As described above, the ROIs vs ROIs correlation heat map (Figure S2a) before Apomorphine exposure indicated that the neural network calcium synchronicity decreases with MMC treatment, a phenomenon that was reversed by treatment with Apomorphine. We observed low synchronous activity in the control group after Apomorphine exposure and the synchronicity gradually increases in VitC to MMC to MMC+VitC group. Exposure to Metoclopramide (Figure 6b) increased peak frequency by 60% (p=0.0096) in control and 30% (p=0.0253) in MMC+VitC groups, but there was no significant changes observed for the VitC and MMC groups. There was also no notable effects observed in the synchronicity of the calcium oscillation before and after treatment with Metoclopramide (Figure S3). Similar effects on calcium peak frequency were observed for Morphine treatment (Figure 6c). There was an increase of 100% (p<0.0001) for control, 24.6% (p=0.0465) for MMC and 40% (p=0.0001) for the MMC+VitC treatment group. There was no statistically significant change observed for VitC treatment group. As seen for the D2-receptor agonist, Morphine, also increased synchronicity in

 doi:10.20944/preprints202205.0256.v1

calcium waves in the MMC+VitC treatment group compared to it control counterpart (Figure S4).

4. Discussion

The advent of iPSC-derived cells has enabled the ability to develop neural cellular models with patient derived cells. In most cases, cells are grown on plastic surfaces coated with exogenously added biopolymers mimicking native ECM to enhance the growth, differentiation and function of the neural cultures. However, these coating do not match the complexity of neural ECM, including various interwoven meshwork of fibrillar proteins such as collagens, glycoproteins like laminins, fibronectin, tenascins, and several classes of proteoglycans (heparan sulfate, chondroitin sulfate, dermatan sulfate, etc) [24, 26, 33]. Therefore, to create more physiologically relevant cellular cultures, it would be more desirable to develop cellular models which synthesize, secrete, and deposit their own native like ECM. This can be achieved by exposing adherent cell cultures to the tissue engineering technique of macromolecular crowding [14]. This technique has been applied successfully in mesenchymal and epithelial cells and tissue equivalents but has been hitherto not been explored in neuronal and neuroglial cells. Here we show that the simultaneous addition of Ficoll 40/700, a known macromolecular crowding agent, and L-ascorbic acid (Vitamin C), a crucial cofactor for collagen secretion, significantly enhances deposition of brain-relevant ECM components by astrocyte monolayer cultures. In this initial experimental design, astrocytes were chosen as targets for the MMC because they are critical for ECM formation in the brain [34]. Mature astrocytes secrete and deposit a wide variety of proteoglycans and extracellular matrix proteins which impact the growth of astrocytes themselves and contributes to the development of neural microenvironment and networks [23]. However, most of what is known on astrocyte ECM production is derived from pathological processes such as glial scar formation and spinal cord injury [35]. The physiological ECM-building capabilities of human astrocyte production *in vitro* have been under researched. We therefore designed our experiments by first pre-treating astrocytes with MMC and VitC to create an ECM bed on which neurons could attach and more effectively establish active functional networks. VitC has long been used in matrix biology to maximize collagen secretion by fibroblasts, but for the exception of Cheng et al (2020), which used it to produce astrocyte matrix, supplementation of neural cultures with VitC appears only rarely in neurobiology literature. We tested several macromolecular crowders, including Dextran sulfate (DxS500kDa), Poly-sodium 4-styrene sulfonate (PSS200kDa), Polyvinylpyrrolidone (PVP360kDa) for these astrocyte cultures. We observed that the largest increase in secretion of collagen IV, fibronectin and laminin (alpha1) was obtained with Ficol40/700. These proteins were chosen because they have been shown to be relevant for formation of neuronal extensions and networks and are detectable by immunostaining. Further work using alternative technologies such as MALDI mass spectrometry will be used to explore depositions of additional ECM proteins and proteoglycans. Our results shows denser ECM proteins deposition by the human astrocytes *in vitro* after MMC treatment. Moreover, when culturing the neurons on top of the MMC-treated astrocytes, the filament-like ECM mesh remarkably aligns itself with mature neurites outgrowth, creating a morphological microenvironment like neural co-cultures in 3D gel-based scaffold (Kundu et al 2022, Manuscript under review).

Work in *C.elegans* suggests that ECM composition surrounding synaptic terminals modulates neuronal morphology and synaptic integrity [36]. In the present study, we established that MMC-enhanced deposition of collagen IV, fibronectin, and laminin in cultured astrocytes, indeed promoted dopaminergic neuronal growth, neurites branching pattern and strengthen of synaptic connections, as evidenced by both pre-synaptic activity and post synaptic density. Previous report shows that laminin at the synaptic cleft modulates synaptic plasticity and controls calcium activity [37]. The effects of the ECM on neural activity could be caused by enhanced synapsis and network formation, as was observed, or by modulation of ions and other factors that affect action potentials. ECM is

 doi:10.20944/preprints202205.0256.v1

the largest source of free calcium ions in the living multicellular organism with 10^4 times higher concentration than cytosol [38] and there are also reports shown that several ECM components can regulate cytosolic calcium levels via mechanotransduction [39]. For example, fibronectin induces cytosolic calcium spikes [40, 41]. Laminin also has calcium binding sites [42] and a recent study shows direct interaction of laminin with voltage-gated calcium channel in neuro-muscular junctions [37, 43]. Lastly, studies using human mesenchymal stem cell culture shows that calcium spikes increase with increasing stiffness of the collagen matrix [44]. These three components of ECM were elevated in our system after MMC and MMC+VitC treatment. We therefore sought to know whether the observed changes in ECM and in network plasticity translated into modulation of neural network functionality. Our data shows that augmented ECM deposition under MMC+VitC treatments increases the frequency of calcium oscillations, while decreasing the overall synchronicity of the neural network *in vitro*. We have also observed low network synchronicity in calcium oscillation in 3D-hydrgel neural cultures using the same iAstros and iDopas (Kundu et al 2022, Manuscript under review), which again would suggest that by using MMC to enhance ECM deposition, we are creating a more three-dimensional (3D)-like microenvironment affecting the intrinsic properties of network connectivity and hence enhancing the complexity of neuronal network toward *in vivo* relevance.

One of the goals of developing physiological relevant cellular models is their use as predictive assays for drug development. Therefore, it is important to establish whether pharmacological responses in cell cultures building their own native ECM are more similar to those seen *in vivo* than those obtained in standard cultures. D2-receptors are abundant on the pre and post synaptic terminals of dopaminergic neurons. They respond to dopamine released by their own nerve ending, thereby negatively modulating the dopaminergic neuronal activity. Thus they function as autocrine inhibitory receptors [45]. *In vivo* studies show that D2 receptor agonist, apomorphine inhibits local field potentials of dopaminergic neurons in rat substantia nigra [46, 47]. In agreement with these results, our study showed that apomorphine reduced calcium oscillations frequency in the MMC+VitC treated conditions. This contrasts with the effects seen in astrocyte-neuron cocultures without prior MMC treatment which showed a positive calcium modulation upon stimulation apomorphine. Therefore, our data suggests that the MMC-enhanced astrocytic ECM microenvironment can make certain pharmacological responses more like *in vivo*. Interestingly, we observed similar pharmacological modulation of calcium activity in iDopas and iAstros coculture system in a 3D fibrinogen gel matrix (Kundu et al 2022, Manuscript under review). Correspondingly, Metoclopramide, a D2 receptor antagonist, had the opposite effects to apomorphine and increased calcium oscillations frequency in the MMC+VitC treatment. On the MMC untreated conditions, though, both Apomorphine and Metoclopramide had the same effect increased calcium oscillations frequency. Overall, our data suggest that the pharmacology of agonists of the dopamine receptor is more native-like in the conditions with the altered ECM secreted by the cultured iPSC derived human astrocytes with the influenced of external macro molecular crowding.

Taken together, utilizing macromolecular crowder in combination with an enhancer of collagen secretion like L-ascorbic acid, we showed that human iPSC derived astrocytes can be induced to deposit more brain relevant extracellular matrix; and that the resultant matrix favors development of iPSC-derived neurons to form active synaptic connections neuronal and enhance neuronal activity, altering the intrinsic physiological property of the neuronal network, in terms of synchronicity. This study provides a glimpse of *in vivo* relevant neuronal modulation *in vitro* when intrinsic matrix formation is facilitated by MMC. This approach is demonstrated in a 96-well plate platform compatible with a high content drug screening format and offers applications with physiological *in vitro* models that more closely mimic properties of the brain *in vivo*.

Author Contributions: MEB, MR and MF conceptualized the project. ANV and SK designed and performed the experiments, collected, and analyzed data; CS produced correlation plots and heat map for single calcium imaging; EL, OJ and MJS contributed intellectually with scientific and technical advice; MF, ANV and SK wrote first draft of manuscript. All the authors contribute to critical reading and editing of manuscript.

Acknowledgments: This study was funded by the NIH Helping to End Addiction Long-Term℠ (HEAL) Initiative and the Cures Acceleration Network at NCATS. We would like to thank other members of the NCATS 3D Tissue Bioprinting Laboratory for their advice during this project.

Conflicts of Interest: The authors declare no conflicts of interest

References

1. Nikolakopoulou, P., et al., *Recent progress in translational engineered in vitro models of the central nervous system.* Brain, 2020. **143**(11): p. 3181-3213.
2. Liang, N., et al., *Stem cell contributions to neurological disease modeling and personalized medicine.* Prog Neuropsychopharmacol Biol Psychiatry, 2018. **80**(Pt A): p. 54-62.
3. Roll, L. and A. Faissner, *Influence of the extracellular matrix on endogenous and transplanted stem cells after brain damage.* Front Cell Neurosci, 2014. **8**: p. 219.
4. Caddeo, S., M. Boffito, and S. Sartori, *Tissue Engineering Approaches in the Design of Healthy and Pathological In Vitro Tissue Models.* Front Bioeng Biotechnol, 2017. **5**: p. 40.
5. Jansen, K.A., et al., *A guide to mechanobiology: Where biology and physics meet.* Biochim Biophys Acta, 2015. **1853**(11 Pt B): p. 3043-52.
6. Baeten, K.M. and K. Akassoglou, *Extracellular matrix and matrix receptors in blood-brain barrier formation and stroke.* Dev Neurobiol, 2011. **71**(11): p. 1018-39.
7. Cabezas, R., et al., *Astrocytic modulation of blood brain barrier: perspectives on Parkinson's disease.* Front Cell Neurosci, 2014. **8**: p. 211.
8. Benarroch, E.E., *Extracellular matrix in the CNS: Dynamic structure and clinical correlations.* Neurology, 2015. **85**(16): p. 1417-27.
9. Galtrey, C.M., et al., *Distribution and synthesis of extracellular matrix proteoglycans, hyaluronan, link proteins and tenascin-R in the rat spinal cord.* Eur J Neurosci, 2008. **27**(6): p. 1373-90.
10. Morawski, M., et al., *Tenascin-R promotes assembly of the extracellular matrix of perineuronal nets via clustering of aggrecan.* Philos Trans R Soc Lond B Biol Sci, 2014. **369**(1654): p. 20140046.
11. Mak, K.M. and R. Mei, *Basement Membrane Type IV Collagen and Laminin: An Overview of Their Biology and Value as Fibrosis Biomarkers of Liver Disease.* Anat Rec (Hoboken), 2017. **300**(8): p. 1371-1390.
12. Thomsen, M.S., L.J. Routhe, and T. Moos, *The vascular basement membrane in the healthy and pathological brain.* J Cereb Blood Flow Metab, 2017. **37**(10): p. 3300-3317.
13. Kajtez, J., et al., *3D biomaterial models of human brain disease.* Neurochem Int, 2021. **147**: p. 105043.
14. Raghunath, M. and D.I. Zeugolis, *Transforming eukaryotic cell culture with macromolecular crowding.* Trends Biochem Sci, 2021. **46**(10): p. 805-811.
15. Lam, D., et al., *Tissue-specific extracellular matrix accelerates the formation of neural networks and communities in a neuron-glia co-culture on a multi-electrode array.* Sci Rep, 2019. **9**(1): p. 4159.
16. Sood, D., et al., *Fetal brain extracellular matrix boosts neuronal network formation in 3D bioengineered model of cortical brain tissue.* ACS Biomater Sci Eng, 2016. **2**(1): p. 131-140.
17. Nakayama, K.H., L. Hou, and N.F. Huang, *Role of extracellular matrix signaling cues in modulating cell fate commitment for cardiovascular tissue engineering.* Adv Healthc Mater, 2014. **3**(5): p. 628-41.
18. Chen, C., et al., *Applying macromolecular crowding to enhance extracellular matrix deposition and its remodeling in vitro for tissue engineering and cell-based therapies.* Adv Drug Deliv Rev, 2011. **63**(4-5): p. 277-90.
19. Ellis, R.J., *Macromolecular crowding: obvious but underappreciated.* Trends Biochem Sci, 2001. **26**(10): p. 597-604.
20. Benny, P. and M. Raghunath, *Making microenvironments: A look into incorporating macromolecular crowding into in vitro experiments, to generate biomimetic microenvironments which are capable of directing cell function for tissue engineering applications.* J Tissue Eng, 2017. **8**: p. 2041731417730467.
21. Benny, P., et al., *Making more matrix: enhancing the deposition of dermal-epidermal junction components in vitro and accelerating organotypic skin culture development, using macromolecular crowding.* Tissue Eng Part A, 2015. **21**(1-2): p. 183-92.
22. Francis, M., et al., *Automated analysis of dynamic Ca2+ signals in image sequences.* J Vis Exp, 2014(88).

23. Sofroniew, M.V., *Molecular dissection of reactive astrogliosis and glial scar formation.* Trends Neurosci, 2009. **32**(12): p. 638-47.
24. Massey, J.M., et al., *Increased chondroitin sulfate proteoglycan expression in denervated brainstem targets following spinal cord injury creates a barrier to axonal regeneration overcome by chondroitinase ABC and neurotrophin-3.* Exp Neurol, 2008. **209**(2): p. 426-45.
25. Quintana, A., et al., *Site-specific production of IL-6 in the central nervous system retargets and enhances the inflammatory response in experimental autoimmune encephalomyelitis.* J Immunol, 2009. **183**(3): p. 2079-88.
26. Kabos, P., et al., *Neural precursors express multiple chondroitin sulfate proteoglycans, including the lectican family.* Biochem Biophys Res Commun, 2004. **318**(4): p. 955-63.
27. Cheng, Y., et al., *Sustained hedgehog signaling in medulloblastoma tumoroids is attributed to stromal astrocytes and astrocyte-derived extracellular matrix.* Lab Invest, 2020. **100**(9): p. 1208-1222.
28. Hynes, R.O., *The extracellular matrix: not just pretty fibrils.* Science, 2009. **326**(5957): p. 1216-9.
29. Zagris, N., et al., *Decorin developmental expression and function in the early avian embryo.* Int J Dev Biol, 2011. **55**(6): p. 633-9.
30. Skeath, J.B., et al., *The extracellular metalloprotease AdamTS-A anchors neural lineages in place within and preserves the architecture of the central nervous system.* Development, 2017. **144**(17): p. 3102-3113.
31. Long, K.R., et al., *Extracellular Matrix Components HAPLN1, Lumican, and Collagen I Cause Hyaluronic Acid-Dependent Folding of the Developing Human Neocortex.* Neuron, 2018. **99**(4): p. 702-719 e6.
32. Long, K.R. and W.B. Huttner, *How the extracellular matrix shapes neural development.* Open Biol, 2019. **9**(1): p. 180216.
33. Quintana, L., N.I. zur Nieden, and C.E. Semino, *Morphogenetic and regulatory mechanisms during developmental chondrogenesis: new paradigms for cartilage tissue engineering.* Tissue Eng Part B Rev, 2009. **15**(1): p. 29-41.
34. Wiese, S., M. Karus, and A. Faissner, *Astrocytes as a source for extracellular matrix molecules and cytokines.* Front Pharmacol, 2012. **3**: p. 120.
35. Yang, T., et al., *Dissecting the Dual Role of the Glial Scar and Scar-Forming Astrocytes in Spinal Cord Injury.* Front Cell Neurosci, 2020. **14**: p. 78.
36. Kurshan, P.T., et al., *Regulation of synaptic extracellular matrix composition is critical for proper synapse morphology.* J Neurosci, 2014. **34**(38): p. 12678-89.
37. Nishimune, H., J.R. Sanes, and S.S. Carlson, *A synaptic laminin-calcium channel interaction organizes active zones in motor nerve terminals.* Nature, 2004. **432**(7017): p. 580-7.
38. Carafoli, E. and J. Krebs, *Why Calcium? How Calcium Became the Best Communicator.* J Biol Chem, 2016. **291**(40): p. 20849-20857.
39. Schwartz, M.A., *Integrins and extracellular matrix in mechanotransduction.* Cold Spring Harb Perspect Biol, 2010. **2**(12): p. a005066.
40. Carbajal, M.E., et al., *Fibronectin-induced intracellular calcium rise in Entamoeba histolytica trophozoites: effect on adhesion and the actin cytoskeleton.* Exp Parasitol, 1996. **82**(1): p. 11-20.
41. Nebe, B., et al., *Mechanical induction of beta 1-integrin-mediated calcium signaling in a hepatocyte cell line.* Exp Cell Res, 1995. **218**(2): p. 479-84.
42. Yurchenco, P.D. and Y.S. Cheng, *Self-assembly and calcium-binding sites in laminin. A three-arm interaction model.* J Biol Chem, 1993. **268**(23): p. 17286-99.
43. Nishimune, H., *Molecular mechanism of active zone organization at vertebrate neuromuscular junctions.* Mol Neurobiol, 2012. **45**(1): p. 1-16.
44. Shih, Y.R., et al., *Matrix stiffness regulation of integrin-mediated mechanotransduction during osteogenic differentiation of human mesenchymal stem cells.* J Bone Miner Res, 2011. **26**(4): p. 730-8.
45. Ford, C.P., *The role of D2-autoreceptors in regulating dopamine neuron activity and transmission.* Neuroscience, 2014. **282**: p. 13-22.
46. Xu, D., et al., *Effects of L-DOPA on nigral dopamine neurons and local field potential: comparison with apomorphine and muscimol.* J Pharmacol Exp Ther, 2011. **337**(2): p. 533-9.
47. Vaglini, F., et al., *Apomorphine offers new insight into dopaminergic neuron vulnerability in mesencephalic cultures.* Neuropharmacology, 2008. **55**(5): p. 737-42.